This is a “preproof” accepted article for *Mineralogical Magazine*.

This version may be subject to change during the production process.

10.1180/mgm.2024.107

Yellowcatite, $KNaFe^{3+}_2(Se^{4+}O_3)_2(V^{5+}_2O_7)\cdot 7H_2O$, the first selenite-vanadate

Anthony R. Kampf[1]*, Travis A. Olds[2], Chi Ma[3] and Joe Marty[1]

[1] Mineral Sciences Department, Natural History Museum of Los Angeles County, 900 Exposition Boulevard, Los Angeles, CA 90007, USA

[2] Section of Minerals and Earth Sciences, Carnegie Museum of Natural History, 4400 Forbes Avenue, Pittsburgh, Pennsylvania 15213, USA

[3] Division of Geological and Planetary Sciences, California Institute of Technology, Pasadena, California 91125, USA

*E-mail: akampf@nhm.org

Abstract

The new mineral yellowcatite (IMA2024-030), $KNaFe^{3+}_2(Se^{4+}O_3)_2(V^{5+}_2O_7)\cdot 7H_2O$, was found underground in the School Section #32 mine, Grand County, Utah, USA, where it is a secondary, post-mining phase occurring on montroseite-corvusite-asphaltite-mica-bearing sandstone in association with barnesite, gypsum and mandarinoite. Crystals are thin hexagonal plates, up to about 0.2 mm in diameter. Crystals are yellow and transparent, with vitreous to pearly lustre and pale-yellow streak. The mineral is brittle with curved fracture and

two cleavages: perfect on {001} and good on {100}. The Mohs hardness is about 2. The measured density is 2.79(2) g·cm^{-3}. Optically, yellowcatite is uniaxial (–) with ω = 1.910(5), ε = 1.740(5) (white light). The mineral is pleochroic with O yellow and E colourless; O > E. The empirical formula is $(K_{0.65}\square_{0.35})_{\Sigma 1.00}(Na_{0.66}Mg_{0.30})_{\Sigma 0.96}Fe^{3+}_{2.02}Se^{4+}_{1.99}V^{5+}_{2.01}O_{20}H_{14.02}$. Yellowcatite is hexagonal, space group *P*-6*m*2, with cell parameters: *a* = 5.4966(7), *c* = 17.2109(16) Å, *V* = 450.31(13) Å^3 and *Z* = 1. In the crystal structure of yellowcatite (R_1 = 5.12% for 281 $I > 2\sigma_I$ reflections), $Fe^{3+}O_6$ octahedra, $Se^{4+}O_3$ pyramids and $V^{5+}O_4$ tetrahedra link by corner-sharing to form sheets similar to those in the well-known merwinite structure, but with the apexes of the $Se^{4+}O_3$ pyramids in the "pinwheels" pointing in the same direction as the $V^{5+}O_4$ tetrahedra. The unshared vertices of the $V^{5+}O_4$ tetrahedra in adjacent sheets link to one another to form divanadate groups, thereby joining two sheets into a double-sheet slab structural unit. Between adjacent slabs is a layer of unlinked $Na(H_2O)_6$ coordinations that are presumed to represent octahedra exhibiting rotational disorder.

Keywords: yellowcatite; new mineral; selenite; divanadate; crystal structure; Raman spectroscopy; School Section #32 mine, Grand County, Utah, USA

Introduction

The sandstone-hosted uranium deposits of the Colorado Plateau are in two distinct mineral systems, one hosted in the Triassic Chinle Formation and the other in the Jurassic Morrison Formation (Hall *et al*., 2023). Both the Chinle and Morrison deposits contain significant amounts of vanadium; however, the Morrison deposits generally contain much more. This is especially true of the deposits in the Uravan mineral belt, a narrow, crescent-shaped area mostly in southwestern Colorado that has historically been one of the most important uranium- and vanadium-producing areas in the United States. A variety of

https://doi.org/10.1180/mgm.2024.107 Published online by Cambridge University Press

"accessory" elements are also found in these deposits. Of particular interest here is selenium. Shoemaker *et al*. (1959) note that Se is more than six times more abundant on average in the uranium ores of the Morrison than in the unmineralized sandstones. They further note that the most Se-rich ores are found northwest of the Colorado River. The deposits in the Thompson district, which is immediately west of the northern end of the Uravan mineral belt (and northwest of the Colorado River), are noteworthy for their high Se contents.

The new selenite-vanadate mineral yellowcatite, described herein, was discovered in the School Section #32 mine, which is in an area in the Thompson district called The Poison Strip. The term "poison strip" has been used by ranchers throughout the region to designate areas containing plants toxic to livestock, and these plants rely on selenium in the soil (Beath, 1943). Cannon (1964) noted that a geochemical halo of uranium, vanadium, selenium, sulfur, arsenic and lead surrounds each orebody. According to Cannon (1964), the selenium accumulator plants *Astragalus pattersoni* (Patterson's milkvetch) and *Astragalus preussii* (Preuss' milkvetch) proved to be especially good indicators of mineralized ground.

Yellowcatite is named for Yellow Cat Mesa on which the School Section #32 mine and other mines in the area are located and for Yellow Cat Road under which the mine tunnel extends. Also, an alternate name for the Thompson district is the Yellow Cat district. The new mineral and the name have been approved by the International Mineralogical Association (IMA2024-030; Warr symbol: Yel). All analyses were conducted on crystals from one holotype (HT) specimen, whereas two cotype (CT) specimens were examined to provide further information on the associated minerals. All three type specimens are deposited in the collections of the Natural History Museum of Los Angeles County, 900 Exposition Boulevard, Los Angeles, CA 90007, USA, catalogue numbers 76356 (HT), 76357 (CT) and 76358 (CT).

https://doi.org/10.1180/mgm.2024.107 Published online by Cambridge University Press

Occurrence

Yellowcatite was found underground in the School Section #32 mine, Thompson district (aka Yellow Cat district), Grand County, Utah, USA (38°51'11"N, 109°30'15"W), about 25 km SE of Thompson Springs and 31 km NNE of Moab. The mine consists of a short tunnel extending under Yellow Cat Road and is about 1.7 km west of the Cactus Rat mine group. Specimens containing yellowcatite were collected in 2006.

Most of the mines in the Thompson district are in the Salt Wash Member of the Jurassic Morrison Formation. Although some reports place the mines of the School Section claims and the Cactus Rat mine group in the basal conglomerate sandy beds of the Brushy Basin Member (just above the Salt Wash Member), Stokes (1952) concluded that they are in the conglomerate at the top of the Salt Wash Member. Cannon (1964) agreed with this placement. The deposits are similar to those of the Uravan mineral belt (Carter and Gualtieri, 1965; Shawe, 2011), which are in the Salt Wash Member.

Yellowcatite occurs on montroseite-corvusite-asphaltite-mica-bearing sandstone in association with barnesite, gypsum, mandarinoite and three as yet unidentified phases. Other minerals that we have identified from the School Section #32 mine include almandine/spessartine, carnotite, cobaltomenite, dzharkenite, ferroselite, gypsum, huemulite, hewettite, jarosite, uvanite(?), a uranyl vanadate that may correspond to synthetic $Na(UO_2)(VO_4)(H_2O)_2$ (PDF 04-018-9705), the possible Na analogue of finchite, an Na-Mg-Al decavanadate similar to pascoite and a phase somewhat similar to sabugalite and threadgoldite. Yellowcatite and other secondary minerals occur as encrustations on mine walls and crystallized under ambient temperatures and generally oxidizing conditions, from water presumably with relatively low pH.

https://doi.org/10.1180/mgm.2024.107 Published online by Cambridge University Press

Physical and optical properties

Yellowcatite crystals are thin hexagonal plates, up to about 0.2 mm long, commonly forming sunburst-like aggregates and tightly intergrown balls (Fig. 1). Crystals exhibit the forms {100} and {001} (Fig. 2). The mineral is yellow and transparent with a pale yellow streak. The mineral does not fluoresce in long- or short-wave ultraviolet light. The Mohs hardness is about 2 based on scratch tests. Crystals are brittle with curved fracture. Cleavage is perfect on {001} and good on {100}. The density measured by flotation in a mixture of methylene iodide and toluene is 2.79(2) $g \cdot cm^{-3}$. The calculated density is 2.780 $g \cdot cm^{-3}$ for the empirical formula and 2.830 $g \cdot cm^{-3}$ for the ideal formula, in both cases using the single-crystal cell. At room temperature, the mineral is insoluble in H_2O and slowly soluble in dilute HCl.

Optically, yellowcatite is uniaxial (–) with indices of refraction $\omega = 1.910(5)$ and $\varepsilon = 1.740(5)$ measured in white light. The mineral is pleochroic with O yellow and E colourless; O > E. The Gladstone-Dale compatibility index, $1 - (K_p/K_c)$, is –0.095 for the empirical formula in the range of poor compatibility (Mandarino, 2007). The unprecedented combination of divanadate and selenite anions could be a factor in the poor compatibility, as could the great difference between ω and ε. The average index of refraction predicted by Gladstone-Dale is 1.779, which is between ω and ε.

Raman spectroscopy

Raman spectroscopy was conducted on a Horiba XploRA PLUS using a 532 nm diode laser, 100 μm slit and 1800 gr/mm diffraction grating and a 100× (0.9 NA) objective. The spectrum from 4000 to 60 cm^{-1} is shown in Figure 2. The 4000 to 1500 cm^{-1} range has been exaggerated to show the weak features in that range.

https://doi.org/10.1180/mgm.2024.107 Published online by Cambridge University Press

The weak broad band from about 3600 to 3100 cm^{-1} with a peak at 3521 cm^{-1} is clearly attributable to OH stretching. Applying the correlation of Libowitzky (1999) reveals that the disordered H_2O groups in yellowcatite form hydrogen bonds ranging between ~2.6 and 3.2 Å (peak = 2.93 Å). According to the X-ray data, these values agree well with the range of likely hydrogen bonds formed between the disordered atoms O5 and O6 (~2.58 to 3.22 Å). The weak band at 1882 cm^{-1} with a shoulder at 1844 cm^{-1} is presumed to be an overtone, probably of the strong band at 950 cm^{-1}. The weak band at 1618 cm^{-1} is consistent with the ν_2 (δ)-bending mode of H_2O groups.

The V and Se atoms in the structure of yellowcatite occupy independent special sites, each with near ideal C_{3v} point symmetry; however, the presence of both $(V^{5+}{}_2O_7)^{4-}$ and $(Se^{4+}O_3)^{2-}$ groups complicates the assignment of bands. The two strong bands at 950 and 808 cm^{-1} likely belong to the symmetric ν_1 mode of each anion, yet their individual assignment is unclear. No known mineral contains both selenite and divanadate oxyanions and the scantly available Raman spectra for chemically related minerals containing just one of these anions (e.g. mandarinoite and volborthite) display wide deviances in the reported positions and assignments of relevant bands. The band positions for $(V^{5+}{}_2O_7)^{4-}$ and $(Se^{4+}O_3)^{2-}$ minerals are strongly dependent on the next-neighbor environment, and the unique arrangement of Fe octahedra binding both selenite and divanadate groups in yellowcatite is likely to blame for these differences. Providing accurate assignments for this mineral will require a combination of calculations and further work in the field and lab to find analogous phases.

Our survey of the 26 $(Se^{4+}O_3)$ mineral spectra available in the RRUFF database (Lafuente *et al*., 2015) show that none of their spectra contain bands (that are specifically attributable to the oxyanion) beyond 900 cm^{-1}. Additionally, in the Raman spectra of decavanadate minerals, strong ν_1 bands occurring near ~980 arise from the short vanadyl (V=O; ~1.77 Å) bonds in the cluster. From this information, we tentatively assign the strong

https://doi.org/10.1180/mgm.2024.107 Published online by Cambridge University Press

band at 950 cm^{-1} to ν_1 $(V^{5+}{}_2O_7)^{4-}$, given the similarly short V–O bonds from the X-ray data (1.69 and 1.78 Å). This band is also composed of a significantly weaker shoulder at 918 cm^{-1}, but we can offer no guidance on its assignment. The moderately intense band at 687 cm^{-1}, with a shoulder near ~705 cm^{-1}, as well as the weak bands at 594, 428 and 361 cm^{-1} likely arise from various stretching or bending modes of the selenite and divanadate groups. Bands at lower wavenumbers are likely attributable to lattice vibrations.

Composition

Electron probe microanalyses (EPMA; 8 points) were performed at Caltech on a JXA-iHP200F electron microprobe in WDS mode. Analytical conditions were 15 kV accelerating voltage, 5 nA beam current and 10 μm beam diameter. No other elements were detected by EDS or WDS. There was significant H_2O loss under vacuum and during analyses resulting in higher concentrations for the remaining constituents than are to be expected for the fully hydrated phase; therefore, the other analyzed constituents have been normalized to provide a total of 100% when combined with the calculated H_2O content. Analytical data are given in Table 1.

The empirical formula based on 1 P and 7 O *apfu* is V + Se = 4 and O = 20 *apfu* is $(K_{0.65}\square_{0.35})_{\Sigma 1.00}(Na_{0.66}Mg_{0.30})_{\Sigma 0.96}Fe^{3+}{}_{2.02}Se^{4+}{}_{1.99}V^{5+}{}_{2.01}O_{20}H_{14.02}$. The simplified formula is $(K,\square)(Na,Mg)Fe^{3+}{}_2(Se^{4+}O_3)_2(V^{5+}{}_2O_7)\cdot 7H_2O$ and the ideal formula is $KNaFe^{3+}{}_2(Se^{4+}O_3)_2(V^{5+}{}_2O_7)\cdot 7H_2O$, which requires K_2O 6.14, Na_2O 4.04, Fe_2O_3 20.80, SeO_2 28.91, V_2O_5 23.69, H_2O 16.43, total 100 wt%.

X-ray crystallography and structure refinement

X-ray powder diffraction data were recorded using a Rigaku R-Axis Rapid II curved imaging plate microdiffractometer with monochromatized Mo*K*α radiation. A Gandolfi-like

https://doi.org/10.1180/mgm.2024.107 Published online by Cambridge University Press

motion on the φ and ω axes was used to randomize the sample. Observed *d*-values and intensities were derived by profile fitting using JADE Pro software (Materials Data, Inc.). The powder data are presented in Table 2. The unit-cell parameters refined from the powder data using JADE Pro with whole-pattern fitting (space group *P*-6*m*2) are a = 5.480(4), c = 17.163(13) Å, V = 446.4(7) Å^3 and Z = 1.

The Rigaku CrystalClear software package was used for processing the structure data, including the application of an empirical absorption correction using the multi-scan method with ABSCOR (Higashi, 2001). The structure was solved using the intrinsic-phasing algorithm of SHELXT (Sheldrick, 2015a). SHELXL-2016 (Sheldrick, 2015b) was used for the refinement of the structure. The V, Se, Fe, O1, O2, O3 and O4 sites were all refined with full occupancies. The Na site refined to an occupancy of 1.01(9), providing a site scattering value of 11.11±0.99*e* as compared to a scattering value of 11.31*e* calculated from the EPMA composition factored to full site occupancy by Na and Mg ($Na_{0.69}Mg_{0.31}$). The K site refined to an occupancy of 0.61(5), not far from the 0.65 occupancy suggested by the EPMA. Two partially occupied O sites (O5 and O6) were located at general positions (12-fold multiplicity) at appropriate distances for coordination to Na at 0,0,0. The distances between these sites and their symmetry equivalents indicate that on average each has an occupancy of 0.25. Refined jointly the occupancy of O5 is 0.22(4) and that of O6 is 0.28(4). Based on this, the Na site has a coordination of six. All sites except O5 and O6 were refined with anisotropic displacement parameters. Difference Fourier syntheses failed to locate H atom positions. Data collection and refinement details are given in Table 3, atom coordinates and displacement parameters in Table 4, selected bond distances in Table 5 and a bond-valence analysis in Table 6.

https://doi.org/10.1180/mgm.2024.107 Published online by Cambridge University Press

Description of the structure

The structure contains $Fe^{3+}O_6$ octahedra, $Se^{4+}O_3$ pyramids and $V^{5+}O_4$ tetrahedra that link by sharing O3 vertices to form a heteropolyhedral double-sheet slab parallel to {001}. Figure 3 shows the linkage of the polyhedra in the {001} plane for one of the sheets in the double-sheet slab, which is similar to that in the well-known merwinite structure (Moore, 1973), but with the apexes of the $Se^{4+}O_3$ pyramids in the "pinwheels" pointing in the same direction as the $V^{5+}O_4$ tetrahedra. The two sheets of the slab are linked *via* a shared vertex between $V^{5+}O_4$ tetrahedra in each sheet, thereby forming a divanadate group at the centre of the double-sheet slab. Open space at the centre of the heteropolyhedral slab hosts K and O4 (H_2O) sites (Figure 4). The K atom bonds to six O2 atoms in the slab at 2.824 Å and three O4 atoms at 3.173 Å. Three O3 sites are also at 3.173 Å from the K site; however, the O3 atom is already bond oversaturated (2.08 *vu*) with bonds to the two V atoms of the divanadate group, so it may not be able to accept additional bond strength from bonds to K. We, therefore, consider K to be nine-fold coordinated, which provides it with a BVS of 1.02 *vu*. Regarding the $Se^{4+}O_3$ pyramid, it is worth noting that its three short Se–O1 bonds are on the side of the Se^{4+} opposite its lone-pair electrons; the Se also forms much longer bonds (closed-shell interactions) with O2 atoms on the same side as its lone-pair electrons.

Between adjacent slabs is a layer of unlinked $Na(H_2O)_6$ coordinations that are presumed to represent octahedra exhibiting rotational disorder about [001]. The O5 and O6 H_2O groups in the $Na(H_2O)_6$ octahedra form hydrogen bonds to the O1 atoms of $Se^{4+}O_3$ pyramids and thereby link the slabs in the [001] direction. The O4 H_2O group may form very long hydrogen bonds to O2 atoms (O4···O2 = 3.612 Å), even though the O2–O3 distance is significantly shorter (3.173 Å) because, as noted above, the O3 atom is already bond oversaturated. Twelve O2 sites are at 3.612 Å from O4 and each O2 site is 3.612 Å from two O2 sites, which results in 2×0.01 *vu* being contributed to O2. Analysis of the hydrogen bonds

https://doi.org/10.1180/mgm.2024.107 Published online by Cambridge University Press

donated by O5 and O6 H_2O groups coordinated to Na is more complex because of the disorder. There are two O5 sites 2.90 Å from O1 and two O6 sites 2.68 Å from O1. It is simplest to consider this as a single hydrogen bond with an average O···O distance of 2.79 Å providing 0.19 *vu* to O1. We further assume that the second hydrogen bond of the O5/O6 H_2O group is to an O5/O6 atom in a different $Na(H_2O)_6$ octahedron. The bond valence donated and accepted for this second O5/O6 H_2O hydrogen bond would thereby be offset and need not be considered in the bond-valence analysis.

Yellowcatite is the first known mineral containing both essential V and Se. It is not closely related structurally to any other known mineral. The only other mineral that contains Fe, Se and O is the ferric selenite mandarinoite, $Fe^{3+}_2(Se^{4+}O_3)_3 \cdot 6H_2O$. In mandarinoite, the $Fe^{3+}O_6$ octahedra and $Se^{4+}O_3$ pyramids link by corner sharing to form a framework, whereas in yellowcatite they link by corner sharing to form a sheet.

Acknowledgements

Structures Editor Peter Leverett, reviewer Mike Rumsey and an anonymous reviewer are thanked for their constructive comments on the manuscript. The EPMA was carried out at the Caltech GPS Division Analytical Facility, which is supported, in part, by NSF Grant EAR-2117942. A portion of this study was funded by the John Jago Trelawney Endowment to the Mineral Sciences Department of the Natural History Museum of Los Angeles County.

References

Beath, O.A. (1943) Toxic vegetation growing on the salt wash sandstone member of the Morrison formation. *American Journal of Botany*, **30**, 698–707.

Cannon, H.L. (1964) *Geochemistry of rocks and related soils and vegetation in the Yellow Cat area, Grand County, Utah* (No. 1176-1179). US Government Printing Office.

https://doi.org/10.1180/mgm.2024.107 Published online by Cambridge University Press

Carter, W.D. and Gualtieri, J.L. (1965) Geology and uranium–vanadium deposits of the La Sal quadrangle, San Juan County, Utah, and Montrose County, Colorado. *United States Geological Survey Professional Paper*, **508**.

Ferraris, G. and Ivaldi, G. (1988) Bond valence vs. bond length in O···O hydrogen bonds. *Acta Crystallographica*, **B44**, 341–344.

Hall, S.M., Van Gosen, B.S. and Zielinski, R.A. (2023) Sandstone-hosted uranium deposits of the Colorado Plateau, USA. *Ore Geology Reviews*, **155**, 105353.

Lafuente, B., Downs, R.T., Yang, H., Stone, N., Armbruster, T. and Danisi, R.M. (2015) The power of databases: the RRUFF project. *Highlights in mineralogical crystallography* **1**, 25.

Libowitzky, E. (1999) Correlation of O–H stretching frequencies and O–H···O hydrogen bond lengths in minerals. *Monatshefte für Chemie*, **130**, 1047–1059.

Mandarino, J.A. (2007) The Gladstone–Dale compatibility of minerals and its use in selecting mineral species for further study. *The Canadian Mineralogist*, **45**, 1307–1324.

Moore, P.B. (1973) Bracelets and pinwheels: A topological-geometrical approach to the calcium orthosilicate and alkali sulfate structures. *American Mineralogist*, **58**, 32–42.

Shawe, D.R. (2011) Uranium-vanadium deposits of the Slick Rock district, Colorado. *United States Geological Survey Professional Paper*, **576-F**.

Stokes, W. L. (1952) Uranium-vanadium deposits of the Thompsons area, Grand County, Utah, with emphasis on the origin of the carnotite ores. *Utah Geological and Mineral Survey Bulletin*, **46**, 51 p.

https://doi.org/10.1180/mgm.2024.107 Published online by Cambridge University Press

FIGURE CAPTIONS

Figure 1. Clusters of yellowcatite hexagonal plates on montroseite-corvusite-asphaltite-mica-bearing sandstone; FOV 0.68 mm across; holotype specimen #76356.

https://doi.org/10.1180/mgm.2024.107 Published online by Cambridge University Press

Figure 2. Raman spectrum of yellowcatite. The spectrum from 400 to 1500 cm^{-1} is shown vertically exaggerated (×50) in inset image.

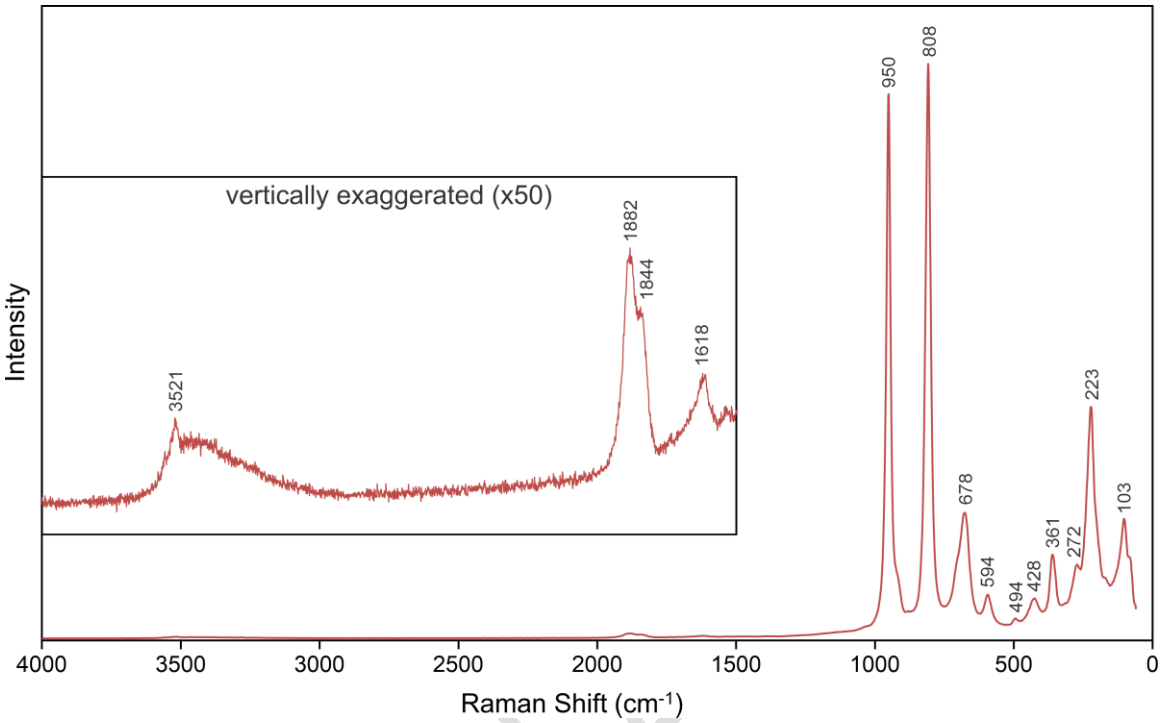

https://doi.org/10.1180/mgm.2024.107 Published online by Cambridge University Press

Figure 3. Half of the heteropolyhedral slab in the structure of yellowcatite viewed along [001].

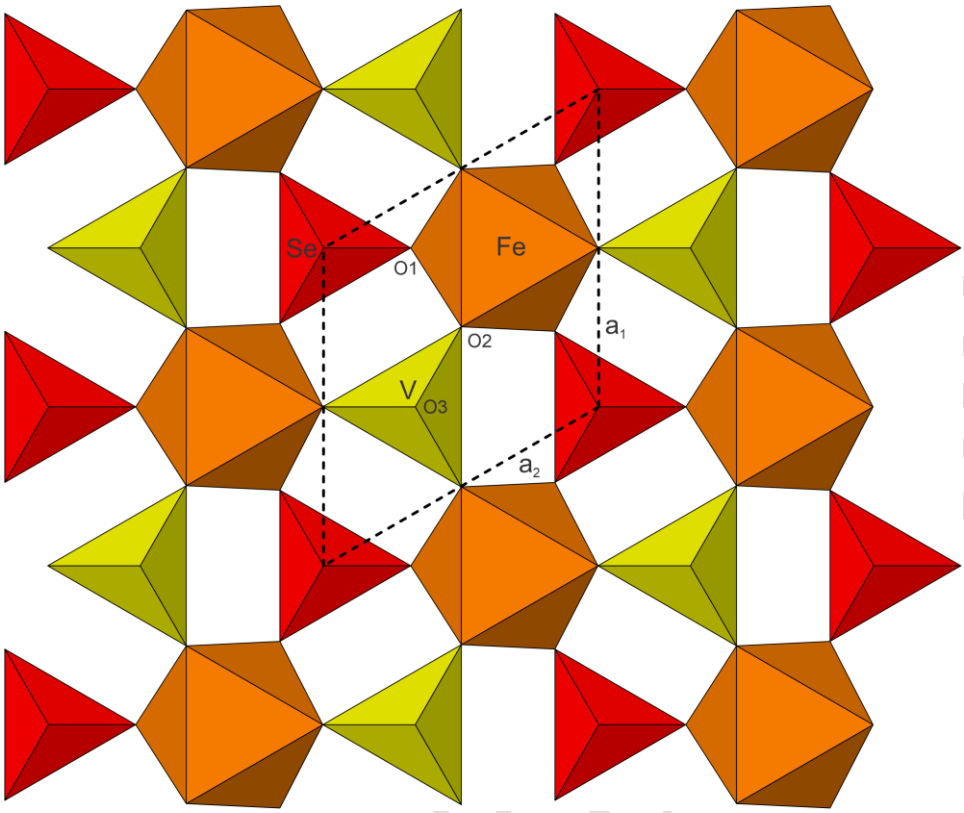

https://doi.org/10.1180/mgm.2024.107 Published online by Cambridge University Press

Figure 4. The structure of yellowcatite viewed along [100]. Unit cell outline is shown with dashed lines.

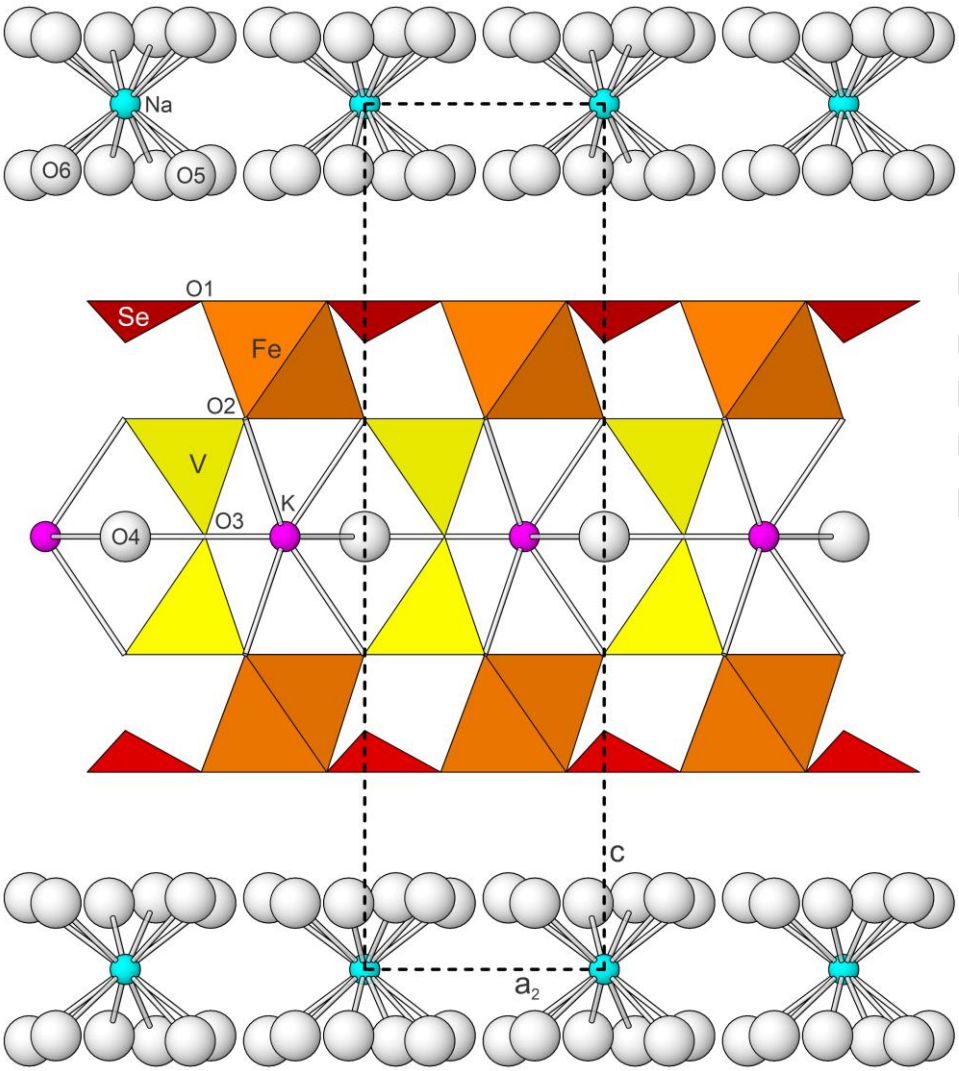

https://doi.org/10.1180/mgm.2024.107 Published online by Cambridge University Press

Table 1. Analytical data (wt%) for yellowcatite.

Constituent	Mean	Range	S.D.	Standard	Normalized
K_2O	4.35	4.24–4.40	0.05	microcline	4.04
Na_2O	2.93	2.82–3.08	0.09	albite	2.72
MgO	1.72	1.68–1.77	0.03	forsterite	1.59
Fe_2O_3	23.03	22.49–23.38	0.28	fayalite	21.38
SeO_2	31.50	31.04–31.91	0.29	Se metal	29.24
V_2O_5	26.15	25.85–26.58	0.22	V_2O_5	24.28
H_2O*	18.05				16.75
Total	**107.73**				100.00

*Based upon the crystal structure with V + Se = 4 and O = 20 *apfu*.

Table 2. Powder X-ray diffraction data (*d* in Å) for yellowcatite.

I_{obs}	d_{obs}	d_{calc}	I_{calc}	*h k l*	I_{obs}	d_{obs}	d_{calc}	I_{calc}	*h k l*
100	17.150	17.211	71	0 0 1	12	1.760	1.761	7	2 1 2
61	8.590	8.606	100	0 0 2			1.721	1	0 0 10
34	5.736	5.737	13	0 0 3	7	1.710	1.710	5	2 0 7
8	4.782	4.760	9	1 0 0			1.694	1	1 1 8
29	4.589	4.588	15	1 0 1	21	1.660	1.660	11	2 1 4
4	4.332	4.303	10	0 0 4	32	1.592	1.595	7	2 1 5
69	4.167	4.165	55	1 0 2			1.587	5	3 0 0
		3.442	1	0 0 5			1.580	1	3 0 1
82	3.193	3.192	55	1 0 4	25	1.570	1.570	10	1 1 9
6	2.864	2.869	6	0 0 6			1.560	1	3 0 2
43	2.777	2.789	12	1 0 5	8	1.529	1.529	2	3 0 3
57	2.730	2.748	22	1 1 0			1.524	1	2 1 6
		2.714	14	1 1 1	8	1.489	1.491	3	2 0 9
14	2.619	2.618	3	1 1 2			1.486	1	1 0 11
16	2.475	2.479	8	1 1 3	9	1.460	1.459	4	1 1 10
		2.457	3	1 0 6	6	1.446	1.452	1	2 1 7
4	2.377	2.380	3	2 0 0			1.441	2	3 0 5
21	2.313	2.316	6	1 1 4			1.395	1	2 0 10
		2.294	1	2 0 2			1.380	1	2 1 8
16	2.195	2.198	7	2 0 3	19	1.376	1.374	9	2 2 0
		2.185	2	1 0 7			1.370	1	2 2 1
14	2.150	2.148	8	1 1 5	9	1.361	1.357	4	2 2 2
21	1.959	1.958	15	2 0 5	10	1.335	1.336	1	2 2 3
5	1.910	1.912	1	0 0 9			1.333	3	3 0 7
30	1.833	1.832	18	1 1 7			1.316	1	3 1 1
		1.799	1	2 1 0	15	1.308	1.307	7	2 0 11
7	1.791	1.789	3	2 1 1			1.305	2	3 1 2

https://doi.org/10.1180/mgm.2024.107 Published online by Cambridge University Press

Table 3. Data collection and structure refinement details for yellowcatite.

Diffractometer	Rigaku R-Axis Rapid II
X-ray radiation / source	Mo$K\alpha$ (λ = 0.71075 Å)
Temperature	293(2)
Formula from SREF	$K_{0.61}Na_{1.01}Fe^{3+}{}_2(Se^{4+}O_3)_2(V^{5+}{}_2O_7)\cdot 7H_2O$ (incl. unlocated H)
Space group	*P*-6*m*2 (#187)
Unit-cell dimensions	*a* = 5.4966(7) Å
	c = 17.2109(16) Å
V	450.31(13) Å^3
Z	1
Density (for above formula)	2.776 g cm^{-3}
Absorption coefficient	6.888 mm^{-1}
F(000)	362.7
Crystal size	50 × 30 × 10 μm
θ range	3.55 to 23.17°
Index ranges	$-6 \le h \le 6$, $-6 \le k \le 6$, $-19 \le l \le 19$
Reflections collected/unique	4661/303; R_{int} = 0.121
Reflections with $I > 2\sigma_I$	281
Completeness to θ = 23.17°	97.8%
Refinement method	Full-matrix least-squares on F^2
Parameter/restraints	42/0
GoF	1.193
Final *R* indices [$I > 2\sigma_I$]	R_1 = 0.0512, wR_2 = 0.1167
R indices (all data)	R_1 = 0.0578, wR_2 = 0.1222
Absolute structure parameter	-0.007(19)
Extinction coefficient	0.015(8)
Largest diff. peak/hole	+1.55/–0.88 e A^{-3}

$R_{int} = \Sigma|F_o^2 - F_o^2(\text{mean})|/\Sigma[F_o^2]$. GoF = $S = \{\Sigma[w(F_o^2 - F_c^2)^2]/(n-p)\}^{1/2}$. $R_1 = \Sigma||F_o| - |F_c||/\Sigma|F_o|$. $wR_2 = \{\Sigma[w(F_o^2 - F_c^2)^2]/\Sigma[w(F_o^2)^2]\}^{1/2}$; $w = 1/[\sigma^2(F_o^2) + (aP)^2 + bP]$ where *a* is 0.0558, *b* is 3.7 and *P* is $[2F_c^2 + \text{Max}(F_o^2, 0)]/3$.

https://doi.org/10.1180/mgm.2024.107 Published online by Cambridge University Press

Table 4. Atom coordinates and displacement parameters (Å^2) for yellowcatite

	x/*a*	*y*/*b*	*z*/*c*	U_{eq}/*U_{iso}	Occupancy	
K	2/3	1/3	1/2	0.027(8)	0.61(5)	
Na	0	0	0	0.024(8)	1.01(9)	
Fe	2/3	1/3	0.2924(3)	0.0188(16)	1	
Se	0	0	0.2753(2)	0.0200(13)	1	
V	1/3	2/3	0.3964(3)	0.0142(15)	1	
O1	0.317(4)	0.159(2)	0.2279(7)	0.023(3)	1	
O2	0.5012(19)	0.4988(19)	0.3638(8)	0.030(3)	1	
O3	1/3	2/3	1/2	0.028(9)	1	
O4	0	0	1/2	0.071(15)	1	
O5*	0.272(8)	0.401(11)	0.083(3)	0.03(2)	0.22(4)	
O6*	0.357(11)	0.290(8)	0.077(2)	0.038(15)	0.28(4)	
	U^{11}	U^{22}	U^{33}	U^{23}	U^{13}	U^{12}
K	0.037(10)	0.037(10)	0.008(11)	0	0	0.018(5)
Na	0.016(8)	0.016(8)	0.040(14)	0	0	0.008(4)
Fe	0.013(2)	0.013(2)	0.031(3)	0	0	0.0063(11)
Se	0.0158(16)	0.0158(16)	0.028(2)	0	0	0.0079(8)
V	0.0137(18)	0.0137(18)	0.015(3)	0	0	0.0068(9)
O1	0.010(7)	0.026(5)	0.027(8)	0.007(3)	0.015(7)	0.005(4)
O2	0.033(6)	0.033(6)	0.032(8)	0.000(5)	0.000(5)	0.024(7)
O3	0.019(10)	0.019(10)	0.05(3)	0	0	0.009(5)
O4	0.05(2)	0.05(2)	0.11(4)	0	0	0.026(10)

Table 5. Selected interatomic distances (Å) in yellowcatite

K–O2 (×6)	2.824(15)	Na–O6 (×3)	2.24(4)	Fe–O2 (×3)	1.998(17)
K–O4 (×3)	3.1734(4)	Na–O5 (×3)	2.41(5)	Fe–O1 (×3)	2.00(2)
K–O3 (×3)	3.1734(4)	<Na–O>	2.32	<Fe–O>	2.00
<K–O>	2.999				
		V–O2 (×3)	1.694(18)	*Hydrogen bonds*	
Se–O1 (×3)	1.716(17)	V–O3	1.783(6)	O4···O3	3.612(9)
Se–O2 (×6)	3.142(7)	<V–O>	1.716	O5···O1	2.90(5)
				O6···O1	2.68(4)

https://doi.org/10.1180/mgm.2024.107 Published online by Cambridge University Press

Table 6. Bond valences (in valence units) for yellowcatite.

	K ×0.61→	Na ($Na_{0.69}Mg_{0.31}$)	Fe^{3+}	V^{5+}	Se^{4+}	H bonds	Σ
O1			$^{\times3\downarrow}$0.52		$^{\times3\downarrow}$1.25	0.19	1.96
O2	$^{\times6\downarrow}$0.14		$^{\times3\downarrow}$0.52	$^{\times3\downarrow}$1.31	$^{\times6\downarrow}$0.04	0.01$^{\times2\rightarrow}$	1.97
O3				1.04$^{\times2\rightarrow}$			2.08
O4	$^{\times3\downarrow}$0.06$^{\times3\rightarrow}$					-0.08$^{\times2\rightarrow}$	-0.04
O5 ×0.22		$^{\times12\downarrow}$0.18$^{\times2\rightarrow}$				-0.19	0.04
O6 ×0.28		$^{\times12\downarrow}$0.27$^{\times2\rightarrow}$					
Σ	1.02	1.38	3.12	4.97	3.99		

Bond–valence parameters are from Gagné and Hawthorne (2015). Hydrogen–bond strengths are based on O–O distances according to the relation of Ferraris and Ivaldi (1988). Negative values indicate donated bond valence. Note the combination of multipliers; for example, there are 12 O5 sites, each 0.22 occupied, that are 2.42 Å from the Na site, their total bond-valence contribute to the Na site is 12 × 0.22 × 0.18 *vu*.

https://doi.org/10.1180/mgm.2024.107 Published online by Cambridge University Press